Trapping Microparticles in a Structured Dark Focus

F. Almeida,[1,*] I. Sousa,[1] O. Kremer,[2] B. Pinheiro da Silva,[3] D. S. Tasca,[3] A. Z. Khoury,[3] G. Temporão,[2] and T. Guerreiro[1,†]

[1]*Departamento de Física, Pontifícia Universidade Católica do Rio de Janeiro, 22451-900 Rio de Janeiro, RJ, Brazil*

[2]*Centro de Estudos em Telecomunicações, Pontifícia Universidade Católica do Rio de Janeiro, 22451-900 Rio de Janeiro, RJ, Brazil*

[3]*Instituto de Física, Universidade Federal Fluminense, Niterói, Rio de Janeiro 24210-346, Brazil*

(Received 7 February 2023; revised 2 May 2023; accepted 11 September 2023; published 17 October 2023)

We experimentally demonstrate stable trapping and controlled manipulation of silica microspheres in a structured optical beam consisting of a dark focus surrounded by light in all directions—the dark focus tweezer. Results from power spectrum and potential analysis demonstrate the nonharmonicity of the trapping potential landscape, which is reconstructed from experimental data in agreement to Lorentz-Mie numerical simulations. Applications of the dark tweezer in levitated optomechanics and biophysics are discussed.

DOI: 10.1103/PhysRevLett.131.163601

Introduction.—Light exerts forces upon matter [1]. As shown by Ashkin [2], these forces can be used to create stable traps for nano- and microscopic dielectric particles, with a myriad of applications from fundamental physics [3–8] to metrology [9–11], quantum information [12,13], and biology [14–16]. When the refractive index of the particle's material is larger than that of its surrounding medium, optical forces attract the object toward high intensities of light. For Gaussian beam optical tweezers, the resulting potential is approximately harmonic [17], and careful calibration of the trap by a number of different methods [18,19] allows for precision force microscopy down to the molecular realm [20].

A growing interest in the fields of levitated optomechanics and optical micromanipulation is in enhanced force effects due to structured materials and light beams. For example, stable Casimir trapping of refractive-index engineered materials [21], enhanced forces in optically active nanocrystals [22] and nitrogen-vacancy color center ensembles [23], and probing of structured beams using levitated nanorods [24] have been demonstrated, while enhanced optical tweezing of meta-atoms exploiting Mie resonances [25], composite microspheres [26], and chiral sorting of microparticles proposed [27,28]. Within this context of engineered nano- and microtraps, we can also explore repulsive optical forces: In the situation that a particle has a lower refractive index than its surrounding medium, it gets expelled from high-intensity regions of light [29]. Using structured beams [30], we can then engineer an inverted optical trap—a dark focal region surrounded by a bright barrier [31]—capable of trapping an object and shielding it from external influence.

A dark focus tweezer (DFT) could find many applications across physics and biology. The optical potential generated by structured light dark traps can have tunable nonharmonicity [32], providing a laboratory for studies of nonlinear stochastic dynamics [17] and non-Gaussian state preparation in optomechanics [33]. Moreover, trapping objects in the dark can be extremely beneficial in the fields of active matter and biophysics, where laser damage limits experiments with living cells [34–36].

In this Letter, we report the construction of a dark optical trap for microparticles as proposed and theoretically analyzed in [32]. Earlier experiments have employed structured light and optical bottle beams to manipulate atoms in blue-detuned lasers [37–40] and micron-sized objects through photophoretic and thermal forces [41]. Here, we demonstrate stable trapping and controlled manipulation of microparticles in a structured light dark focus through optical forces alone. As we will show, the DFT induces a strongly nonharmonic potential landscape reflected as non-Gaussianity in the statistical properties of the particle's stochastic trajectory. We probe the particle motion through both its power spectrum density as well as potential analysis and reconstruct the optical potential landscape through matching of data with numerical simulations.

The dark focus tweezer.—The DFT, sometimes also called the optical bottle beam [31], consists of a dark focus surrounded by a bright intensity region [32]. There are different ways of generating a DFT [42–46]; for simplicity, we choose a superposition of a Gaussian ($\ell = 0$, $p = 0$) with a Laguerre-Gauss (LG) beam ($\ell = 0$, $p = 1$) with a relative phase of π [32]. This choice for a bottle beam allows for an intuitive description of the optical potential and can be readily generated using a spatial light modulator (SLM).

For a DFT of wavelength λ_0 in a medium of refractive index n_m, the most important parameter is the numerical aperture NA, from which the beam waist $\omega_0 = \lambda_0/\pi\mathrm{NA}$

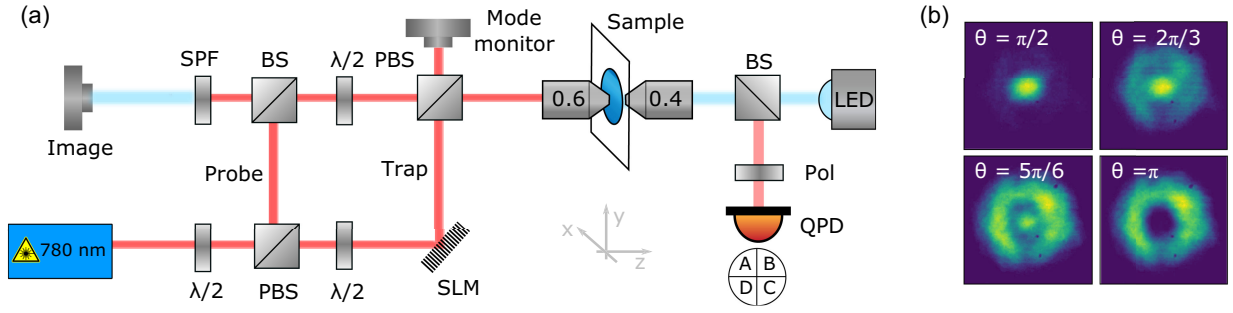

FIG. 1. (a) Simplified setup: A 780 nm cw laser is split into orthogonal polarizations by a half wave plate ($\lambda/2$) and a polarizing beam splitter (PBS). The vertically polarized beam (trap) is modulated by an SLM and directed to an objective (NA = 0.6) to generate the optical trap. The horizontal component (probe) traverses the trap and is collected by a second objective (NA = 0.4) and used to probe the motion of a trapped microparticle with a QPD. The trapping beam is filtered by a polarizer (pol). The image of the trapped particle is obtained by focusing light from a LED onto the particle, subsequently collected by the trapping objective, filtered by a short pass filter (SPF), and focused onto a CCD (image). (b) Behavior of the intensity distribution around the focal point can be mimicked by varying the relative phase θ between the Gaussian and LG modes.

and Rayleigh range $z_R = n_m\lambda_0/\pi \mathrm{NA}^2$ can be calculated. The total average intensity of the beam is $I_0 = 2P_0/\pi\omega_0^2$, where P_0 is the total beam power. We can also define the width W and height H of the bottle as the distances between the peak values of intensity along the x and z directions; these are $W = 2\omega_0$ and $H = 2z_R$, from which we see that the width scales as NA^{-1} and height as NA^{-2} (see Supplemental Material [47]).

For a particle of radius much smaller than the beam wavelength, $R \ll \lambda_0$, optical forces due to a linearly polarized light beam are decomposed into scattering (nonconservative) and gradient (conservative) components, both increasing with the factor $\alpha = [(m^2-1)/(m^2+2)]$, where $m = n_p/n_m$ is the particle-medium refractive index ratio. We are interested in situations where $m < 1$ (i.e., $n_p < n_m$) and the particles are repelled by higher intensities of light [48]. The gradient force field can be expressed in terms of the potential landscape:

$$V(\vec{r}) = -\frac{2\pi n_m R^3}{c}\alpha I(\vec{r}), \tag{1}$$

where $I(\vec{r})$ is the beam intensity at position $\vec{r}$. Note that the potential may switch from attractive to repulsive depending on the value of m; although our experimental conditions do not fit the dipole regime, this feature remains valid in our experiment. As discussed in [32], near the origin (i.e., $\rho \ll \omega_0$, $z \ll z_R$), the potential $V(\vec{r})$ can be expanded as a polynomial function of coordinates:

$$V(\rho, z) \approx \frac{k_z}{2}z^2 - k_{\rho z}\rho^2 z^2 + \frac{k_\rho}{4}\rho^4, \tag{2}$$

where k_z is the harmonic term strength along the axial direction and $k_{\rho z}$ and k_ρ denote the anharmonic potential strengths. In the Rayleigh regime, these potential coefficients are simple functions of the beam parameters (see Supplemental Material [47]) [32].

In our experiment, trapped particles have a radius of $R = 575$ nm, comparable to the wavelength $\lambda_0 = 780$ nm, a regime in which generalized Lorentz-Mie scattering theory must be employed for the calculation of optical forces [49]. Numerical simulation of the resulting force fields can be performed using the toolbox presented in [50]. Equation (2) provides a good approximation to the potential landscape near the origin also in the intermediate regime, with root-mean-square deviations with respect to full numerical simulation of Lorentz-Mie scattering theory below 1% for a wide range of particle radii (see Supplemental Material [47]).

Experimental setup.—The experimental setup for generating a dark focus tweezer can be seen in Fig. 1(a). A cw laser at 780 nm (Toptica DL-pro) seeds a tapered amplifier (Toptica BoosTa) yielding 1.6 W of power. The beam is divided by a half wave plate and a polarizing beam splitter (PBS) to produce the trapping beam and an auxiliary probe beam. The trapping beam is modulated by an SLM (Holoeye) and sent through an objective (Olympus UPlanFLN 100× adjustable NA = 0.6–1.3). The resulting superposition can be monitored in a camera providing a visualization of the beam's transverse profile as shown in Fig. 1(b). We change the relative phase between the modes in order to mimic the DFT's intensity pattern along the axial direction. The image of the trapped particle is produced by focusing light from a LED into the sample, subsequently collecting it with the trapping objective, and projecting onto a CCD (image camera).

SiO_2 beads of radius $R = 575$ nm (microParticles GmbH) with refractive index $n_p = 1.45$ are immersed in clover oil solution, with a refractive index of $n_m = 1.53$ and measured transmission for 780 nm of $\eta_{\mathrm{clover}} = 85\%$. To load the trap, we position the center of the beam at the location of a nanoparticle and abruptly turn on the dark focus tweezer. The hydrophobic nature of the oil increases

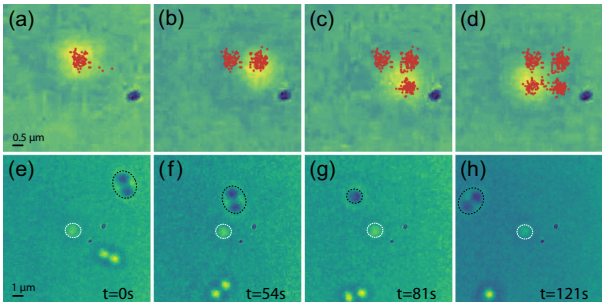

FIG. 2. (a)–(d) Controlled SLM motion of the trapped particle. Position is tracked by monitoring the coordinate of the brightest pixel. (e)–(h) Shielding effect: A dumbbell (black contour) is repelled after approaching a trapped particle (white contour). See supplemental videos [47].

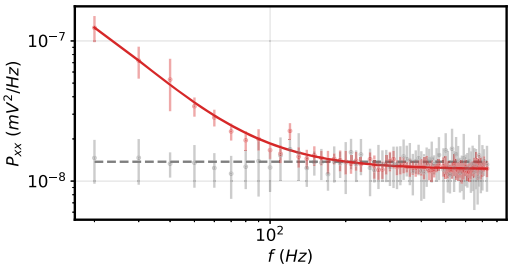

FIG. 3. PSD of a particle trapped in the dark focus (red line) in comparison to background noise (gray line). The effective corner frequency is $f_{c,\mathrm{DFT}} = (13.4 \pm 0.7)$ Hz.

the tendency of the silica microspheres to aggregate, occasionally forming microdumbbells in addition to single particles.

Controlled particle motion and shielding.—As a first demonstration of stable trapping in the DFT, we slightly move the beam by adjusting the SLM modulation angle, allowing for a fine control of the particle position by deflecting the dark focus center. Figures 2(a)–2(d) show the iteration of four different trap positions, with red dots marking the brightest pixel in the image approximately corresponding to the center of the microsphere; see Supplemental Video S1 [47]. These images are obtained by collecting the light from an LED scattered by the particle and registered with the CCD camera, as shown in Fig. 1. By switching off the Gaussian component of the DFT superposition and producing a pure LG mode, we observed the particle is lost from the trap.

In Gaussian optical tweezers, additional objects in the sample traveling near the trapped particle are drawn into the potential landscape by the attractive optical forces. In contrast, a particle trapped in the DFT is shielded from the influence of these external objects due to the repulsive optical force. Figures 2(e)–2(h) display typical subsequent frames of a trapped particle (white dotted circle) surrounded by free, passing-by particles. We observe a microdumbbell (black dashed circle) approaching the trapped particle and subsequently repelled by the DFT beam; see Supplemental Video S2 [47].

Power spectrum analysis.—Among the most employed techniques to calibrate optical traps [51,52] is the power spectrum density analysis (PSD). Analysis of the Langevin equation for a trapped particle in a harmonic potential reveals that the PSD has a Lorentzian form with the corner frequency parameter proportional to the trap's stiffness [53].

The potential associated to the DFT can be modeled by a fourth-order polynomial in the particle's coordinates, thus being nonharmonic (see Supplemental Material [47]). Numerical simulations of a trapped particle in the overdamped regime subject to quartic potentials show that the PSD of the particle motion is well fitted by a Lorentzian function, despite the exact relation between the corner frequency and the trap's strength parameters being unknown beyond perturbation theory [17]. In effect, the PSD method cannot be directly used to determine the DFT's strength constants, but we can use it as a consistency check between numerical simulations of the particle motion subject to optical forces in the intermediate regime and experimental data. This indirectly provides information on the trap's characteristics.

Because of the nature of the dark trap, scattering of photons is greatly reduced, hindering motion detection by the traditional technique of collecting light scattered from the trapping beam [54]. To overcome this, we employ an auxiliary weak *probe beam* in a Gaussian mode with polarization orthogonal to the trapping beam. Being distinguishable and provided it has low power, the probe beam does not significantly alter the properties of the dark trap. Moreover, any eventual residual scattering noise due to the trapping beam can be filtered by a suitably aligned polarizer before detection, allowing access to the information carried by the probe alone. The probe light scattered by the particle is collected by a second objective lens (Olympus PlanN 10×, NA = 0.25) and directed to a quadrant photodetector (QPD, New Focus 2931) generating signals proportional to the particle's radial and axial coordinates (see Supplemental Material [47] for details).

We now turn to measurements of the PSD of a particle trapped in the dark focus. The measured PSD can be seen in Fig. 3 (red dots and line) together with the background scattering noise in the absence of a trapped particle (gray dots and line), for comparison. A Lorentzian fit to the PSD yields an effective corner frequency of $f_{c,\mathrm{DFT}} = (13.4 \pm 0.7)$ Hz. Numerical simulations of the trapped particle within the DFT suggests that this value lies in the NA range between 0.46 and 0.49, where we find corner frequencies in the range between $f_{c,\mathrm{sim}} = (12.6 \pm 2.3)$ Hz and $f_{c,\mathrm{sim}} = (19.2 \pm 7.3)$ Hz, respectively. Using the scaling of width W and height H with the NA introduced earlier, we estimate the order-of-magnitude of the trap size to lie between 1.0 and 1.1 μm. Considering that our particles have a diameter of 1.15 μm, this suggests the view that the trapped particle feels only loose forces within the dark focal region.

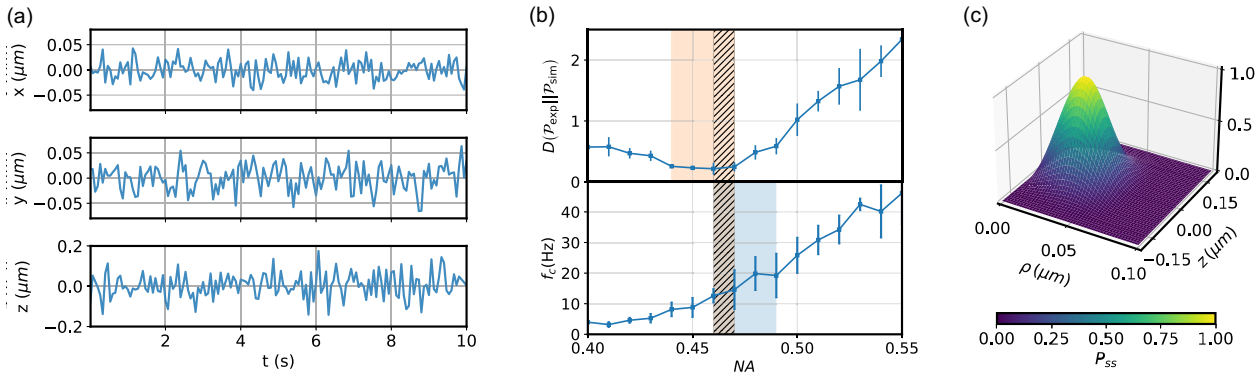

FIG. 4. Potential analysis. (a) Position traces of the particle. (b) Top: Kullback-Leibler divergence $D(\mathcal{P}_{\mathrm{exp}}\|\mathcal{P}_{\mathrm{sim}})$ between simulation and experiment as a function of the NA. The orange region displays the range in which simulated and experimental probability distributions are most similar. Bottom: corner frequency of simulated dynamics. The blue region displays the range where the effective corner frequency of the simulation is within the error margin of measured value $f_{c,\mathrm{DFT}} = (13.4 \pm 0.7)$ Hz. The hatched area shows the intersection of both methods, NA = 0.46–0.47. (c) Fitted normalized PDF of the centroid's position.

Potential analysis.—In thermal equilibrium and in the limit that the conservative force dominates over dissipative forces, the position probability density function (PDF) follows $P(\rho, z) \propto \exp\left(-V(\rho, z)/k_B T\right)$ and can be reconstructed from frames of the particle motion acquired with a CCD over long times [51]. We acquired long-duration videos of a trapped particle at a rate of 15.0 frames/s, from which we extract the particle's centroid and axial coordinates using image processing [55]. The resulting coordinate traces can be seen in Fig. 4(a). Because of the potential anharmonicity, the position PDF is expected to be non-Gaussian; a Kolmogorov-Smirnov hypothesis test on the position time series confirms that at 0.05 significance.

To find the best match between the data and the quartic potential model, we ran several simulations of the particle dynamics in the DFT parametrized by the trap's NA. We then extract simulated PDFs for motion along the transverse directions and numerically compute the Kullback-Leibler (KL) divergence between each of the simulated distributions and the marginal PDFs obtained from the experiment. Minimizing the KL divergence between simulation and experiment is equivalent to performing a maximum likelihood estimation of the trap's NA [56]. Figure 4(b) displays the KL divergence averaged over the x and y directions (top plot), where we find that a potential with NA = 0.46 best describes the measured position traces, consistent with the expectation from Gaussian optics provided the beam waist prior to the SLM, given by NA ≤ 0.6. Moreover, we compute the PSD of the numerical simulations' position data, from which we obtain the corner frequency of the Lorentzian fit. The obtained values of corner frequency for each simulation are plotted as a function of NA in Fig. 4(b) (bottom plot), where we see that NA = 0.46 also displays the best agreement with the PSD measurements, $f_{c,\mathrm{sim}} = (12.6 \pm 2.3)$ Hz.

From the position traces, we can reconstruct the PDF, which is fitted according to the equilibrium prediction. The resulting fit is seen in Fig. 4(c). Proper calibration of the transverse directions is achieved through independent measurements of the CCD's pixel size compared to a reference, while the longitudinal direction is measured by integrating the image brightness over the trapped sphere [54], and calibrated via comparing the root-mean-square deviations of the matched simulation with the measured

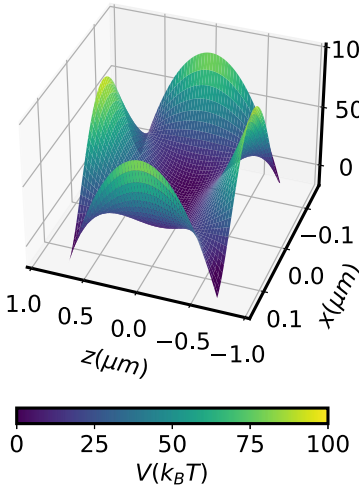

FIG. 5. Reconstructed potential for centroid coordinate of a particle in the DFT.

TABLE I. Reconstructed potential parameters in comparison to numerical simulations of Lorentz-Mie theory. Error bars are obtained by dividing the experimental and simulated data into five sets and taking the standard deviation.

Parameter	Experiment	Lorentz-Mie simulation
k_z (N/m)	$(3.86 \pm 0.06) \times 10^{-7}$	$(2.93 \pm 0.79) \times 10^{-7}$
$k_{\rho z}$ (N/m^3)	$(8.81 \pm 0.14) \times 10^{7}$	$(8.84 \pm 0.25) \times 10^{7}$
k_{ρ} (N/m^3)	$(2.26 \pm 0.07) \times 10^{8}$	$(1.63 \pm 0.17) \times 10^{8}$

data. The reconstructed potential at the trapped sphere's centroid position—obtained by taking the logarithm of the PDF—is shown in Fig. 5, with the corresponding parameters obtained from the experiment and in comparison to full Lorentz-Mie numerical simulation of a DFT with NA = 0.46 in Table I.

Conclusion.—In summary, we have experimentally investigated a structured light dark focus tweezer for dielectric microparticles immersed in a high refractive index medium. We have shown stable trapping and isolation from surrounding objects by repulsive optical forces, which induce a nonharmonic potential landscape.

We expect the dark trap will find use in both applied and fundamental physics. In biophysics, dark tweezers can provide stable trapping for organisms with reduced laser heating. This is advantageous, as it has been shown that bright tweezers hinder cell reproduction and exponentially decrease cell lifetime even at modest trapping powers [57]. Moreover, the dark focus tweezer can be used for vacuum optical trapping using doped nanoparticles, for instance, with rare-earth atoms [22] or Mie particles [25]. Note that implementing a vacuum dark tweezer requires advancements in material science. Optical absorption by particles with internal resonances typically leads to unstable dynamics and particle loss caused by spectral and geometrical imperfections. If these challenges can be overcome, the dark focus tweezer could provide the advantage of a significantly reduced internal bulk temperature of the particle, consequently reducing the decoherence effects caused by thermal emission.

Code and data are available at GitHub [58].

We acknowledge Bruno Melo, Igor Brandão, Marcelo Huguenin, Cyril Laplane, and Lukas Novotny for helpful discussions and Angela Duncke for help on the sample preparation protocol. Conselho Nacional de Desenvolvimento Científico e Tecnológico (CNPq), Coordenação de Aperfeiçoamento de Pessoal de Nível Superior (CAPES), Fundação Carlos Chagas Filho de Amparo à Pesquisa do Estado do Rio de Janeiro (FAPERJ), Instituto Nacional de Ciência e Tecnologia de Informação Quântica (INCT-IQ 465469/2014-0), and Fundação de Amparo à Pesquisa do Estado de São Paulo (FAPESP, Processos No. 2021/06823-5 and No. 2021/06736-5).

*felipealmeida@aluno.puc-rio.br
†barbosa@puc-rio.br

[1] R. A. Beth, Phys. Rev. **50**, 115 (1936).
[2] A. Ashkin, Proc. Natl. Acad. Sci. U.S.A. **94**, 4853 (1997).
[3] U. Delić, M. Reisenbauer, K. Dare, D. Grass, V. Vuletić, N. Kiesel, and M. Aspelmeyer, Science **367**, 892 (2020).
[4] D. Windey, C. Gonzalez-Ballestero, P. Maurer, L. Novotny, O. Romero-Isart, and R. Reimann, Phys. Rev. Lett. **122**, 123601 (2019).
[5] L. Magrini, P. Rosenzweig, C. Bach, A. Deutschmann-Olek, S. G. Hofer, S. Hong, N. Kiesel, A. Kugi, and M. Aspelmeyer, Nature (London) **595**, 373 (2021).
[6] J. Rieser, M. A. Ciampini, H. Rudolph, N. Kiesel, K. Hornberger, B. A. Stickler, M. Aspelmeyer, and U. Delić, Science **377**, 987 (2022).
[7] C. P. Blakemore, D. Martin, A. Fieguth, N. Priel, G. Venugopalan, A. Kawasaki, and G. Gratta, Phys. Rev. A **106**, 023503 (2022).
[8] G. Afek, D. Carney, and D. C. Moore, Phys. Rev. Lett. **128**, 101301 (2022).
[9] S. Barzanjeh, A. Xuereb, S. Gröblacher, M. Paternostro, C. A. Regal, and E. M. Weig, Nat. Phys. **18**, 15 (2022).
[10] F. Ricci, M. T. Cuairan, A. W. Schell, E. Hebestreit, R. A. Rica, N. Meyer, and R. Quidant, ACS Nano **16**, 8677 (2022).
[11] M. Asano, H. Yamaguchi, and H. Okamoto, Sci. Adv. **8**, eabq2502 (2022).
[12] N. Fiaschi, B. Hensen, A. Wallucks, R. Benevides, J. Li, T. P. M. Alegre, and S. Gröblacher, Nat. Photonics **15**, 817 (2021).
[13] O. Houhou, D. W. Moore, S. Bose, and A. Ferraro, Phys. Rev. A **105**, 012610 (2022).
[14] H. M. Nussenzveig, Eur. Biophys. J. **47**, 499 (2018).
[15] G. R. d. S. Araújo, N. B. Viana, F. Gómez, B. Pontes, and S. Frases, Cell surface reviews **5**, 100028 (2019).
[16] C. J. Bustamante, Y. R. Chemla, S. Liu, and M. D. Wang, Nat. Rev. Methods Primers **1**, 1 (2021).
[17] B. Suassuna, B. Melo, and T. Guerreiro, Phys. Rev. A **103**, 013110 (2021).
[18] L. Pérez García, J. Donlucas Pérez, G. Volpe, A. V Arzola, and G. Volpe, Nat. Commun. **9**, 1 (2018).
[19] J. Gieseler, J. R. Gomez-Solano, A. Magazzù, I. P. Castillo, L. P. García, M. Gironella-Torrent, X. Viader-Godoy, F. Ritort, G. Pesce, A. V. Arzola *et al.*, Adv. Opt. Photonics **13**, 74 (2021).
[20] C. Bustamante and S. Yan, Q. Rev. Biophys. **55**, e9 (2022).
[21] R. Zhao, L. Li, S. Yang, W. Bao, Y. Xia, P. Ashby, Y. Wang, and X. Zhang, Science **364**, 984 (2019).
[22] X. Shan, F. Wang, D. Wang, S. Wen, C. Chen, X. Di, P. Nie, J. Liao, Y. Liu, L. Ding *et al.*, Nat. Nanotechnol. **16**, 531 (2021).
[23] M. L. Juan, C. Bradac, B. Besga, M. Johnsson, G. Brennen, G. Molina-Terriza, and T. Volz, Nat. Phys. **13**, 241 (2017).
[24] Y. Hu, J. J. Kingsley-Smith, M. Nikkhou, J. A. Sabin, F. J. Rodríguez-Fortuño, X. Xu, and J. Millen, Nat. Commun. **14**, 2638 (2023).
[25] S. Lepeshov, N. Meyer, P. Maurer, O. Romero-Isart, and R. Quidant, Phys. Rev. Lett. **130**, 233601 (2023).
[26] R. Ali, F. A. Pinheiro, R. S. Dutra, and P. A. Maia Neto, Phys. Rev. A **102**, 023514 (2020).
[27] R. Ali, F. Pinheiro, R. Dutra, F. Rosa, and P. M. Neto, J. Opt. Soc. Am. B **37**, 2796 (2020).
[28] R. Ali, R. Dutra, F. Pinheiro, and P. M. Neto, Opt. Lett. **46**, 1640 (2021).
[29] A. Ashkin, Phys. Rev. Lett. **24**, 156 (1970).
[30] Y. Yang, Y. Ren, M. Chen, Y. Arita, and C. Rosales-Guzmán, Adv. Opt. Photonics **3**, 034001 (2021).

[31] J. Arlt and M. J. Padgett, Opt. Lett. **25**, 191 (2000).
[32] B. Melo, I. Brandão, B. P. da Silva, R. Rodrigues, A. Z. Khoury, T. Guerreiro, and T. Guerreiro, Phys. Rev. Appl. **14**, 034069 (2020).
[33] L. Neumeier, M. A. Ciampini, O. Romero-Isart, M. Aspelmeyer, and N. Kiesel, arXiv:2207.12539.
[34] H. Zhang and K.-K. Liu, J. R. Soc. Interface **5**, 671 (2008).
[35] A. Ehrlicher, T. Betz, B. Stuhrmann, D. Koch, V. Milner, M. Raizen, and J. Käs, Proc. Natl. Acad. Sci. U.S.A. **99**, 16024 (2002).
[36] A. Blázquez-Castro, Micromachines **10**, 507 (2019).
[37] L. Isenhower, W. Williams, A. Dally, and M. Saffman, Opt. Lett. **34**, 1159 (2009).
[38] P. Xu, X. He, J. Wang, and M. Zhan, Opt. Lett. **35**, 2164 (2010).
[39] D. Barredo, V. Lienhard, P. Scholl, S. de Léséleuc, T. Boulier, A. Browaeys, and T. Lahaye, Phys. Rev. Lett. **124**, 023201 (2020).
[40] P. Zhang, Z. Zhang, J. Prakash, S. Huang, D. Hernandez, M. Salazar, D. N. Christodoulides, and Z. Chen, Opt. Lett. **36**, 1491 (2011).
[41] L. Gong, W. Liu, Q. Zhao, Y. Ren, X. Qiu, M. Zhong, and Y. Li, Sci. Rep. **6**, 1 (2016).
[42] D. Yelin, B. E. Bouma, and G. J. Tearney, Opt. Lett. **29**, 661 (2004).
[43] T. Du, T. Wang, and F. Wu, Opt. Commun. **317**, 24 (2014).
[44] M.-D. Wei, W.-L. Shiao, and Y.-T. Lin, Opt. Commun. **248**, 7 (2005).
[45] Z. Yang, X. Lin, H. Zhang, X. Ma, Y. Zou, L. Xu, Y. Xu, and L. Jin, Appl. Opt. **58**, 2471 (2019).
[46] G. Whyte and J. Courtial, New J. Phys. **7**, 117 (2005).
[47] See Supplemental Material at http://link.aps.org/supplemental/10.1103/PhysRevLett.131.163601 for detailed descriptions of the dark focus mode functions, potential analysis, probe beam calibration and reduced absorbed power in the dark focus tweezer.
[48] G. Grynberg, A. Aspect, and C. Fabre, *Introduction to Quantum Optics: From the Semi-Classical Approach to Quantized Light* (Cambridge University Press, Cambridge, England, 2010).
[49] P. Jones, O. Maragó, and G. Volpe, *Optical Tweezers* (Cambridge University Press, Cambridge, England, 2015).
[50] T. A. Nieminen, V. L. Loke, A. B. Stilgoe, G. Knöner, A. M. Brańczyk, N. R. Heckenberg, and H. Rubinsztein-Dunlop, J. Opt. A **9**, S196 (2007).
[51] J. Gieseler, J. R. Gomez-Solano, A. Magazzù, I. P. Castillo, L. P. García, M. Gironella-Torrent, X. Viader-Godoy, F. Ritort, G. Pesce, A. V. Arzola, K. Volke-Sepúlveda, and G. Volpe, Adv. Opt. Photonics **13**, 74 (2021).
[52] B. Melo, F. Almeida, G. Temporão, and T. Guerreiro, Opt. Express **28**, 16256 (2020).
[53] K. Berg-Sørensen and H. Flyvbjerg, Rev. Sci. Instrum. **75**, 594 (2004).
[54] F. Tebbenjohanns, M. Frimmer, and L. Novotny, Phys. Rev. A **100**, 043821 (2019).
[55] D. A. Forsyth and J. Ponce, *Computer Vision: A Modern Approach* (Prentice Hall Professional Technical Reference, Boston, 2002).
[56] J. A. Rice, *Mathematical Statistics and Data Analysis* (China Machine Press, Shanghai, 2003).
[57] Z. Pilát, A. Jonáš, J. Ježek, and P. Zemánek, Sensors **17**, 2640 (2017).
[58] F. Almeida, I. Sousa, O. Kremer, and T. Guerreiro Repository, 10.5281/zenodo.8380357.